Title
EXPERIMENTS ON ALFVEN-WAVE PROPAGATION

Authors
Wilcox, John M.
DeSilva, Alan W.
Cooper, William S.

Publication Date
1961-05-10

UCRL-9613

UNIVERSITY OF CALIFORNIA

Ernest O. Lawrence Radiation Laboratory

BERKELEY, CALIFORNIA

DISCLAIMER

UCRL-9613
Limited distribution

UNIVERSITY OF CALIFORNIA
Lawrence Radiation Laboratory
Berkeley, California

Contract No. W-7405-eng-48

EXPERIMENTS ON ALFVÉN-WAVE PROPAGATION

John M. Wilcox, Alan W. DeSilva, and William S. Cooper, III

May 10, 1961

EXPERIMENTS ON ALFVÉN-WAVE PROPAGATION

John M. Wilcox, Alan W. DeSilva, and William S. Cooper, III

Lawrence Radiation Laboratory
University of California
Berkeley, California

May 10, 1961

ABSTRACT

The propagation of torsional hydromagnetic (Alfvén) waves in a cylindrical hydrogen plasma is discussed. The hydromagnetic waveguide consists of a copper cylinder 86 cm long and 15 cm in diameter, filled with hydrogen to a pressure of 100 μ and immersed in a uniform axial magnetic field of 16 kgauss. The waveguide is filled with plasma by an interesting type of switch-on ionizing wave that produces a high degree of ionization (80 to 100%) and a temperature of about 10,000° K. Ion densities have been measured with an accuracy of about ±15% by observing with a monochromator the profiles of the first three Balmer lines and comparing with a more exact theory of Stark broadening developed by Griem, Kolb, and Shen. The ion density decreases by a factor of three in 300 μsec because of recombination and diffusion losses.

After the waveguide is filled with plasma, a torsional hydromagnetic wave is induced by discharging a 0.2-μf capacitor between the copper cylinder and a small coaxial electrode mounted in a pyrex insulator at one end of the guide. The Alfvén velocity is $V_A = B/(\mu_0 \rho)^{1/2}$. Inserting the spectroscopic measurement of ion density and the known value of axial magnetic field into this expression yields a wave velocity in agreement with experiment. The observed radial distribution of the wave magnetic field is consistent with the first-order Bessel function predicted by theory. The amplitude of a wave that has made one transit of the waveguide agrees within 15% with the value calculated from the amount of energy stored in the 0.2-μf capacitor that drives the wave. Wave reflections have been observed from a high-impedance boundary (a pyrex plate at the end of the guide), from a low-impedance boundary (a copper plate), and from a plasma-neutral gas interface. In all cases, the change in phase of the electric and magnetic fields of the reflected wave agrees with theory. Two different types of measurement indicate that the decaying plasma is electrically isolated from the (conducting) walls.

EXPERIMENTS ON ALFVÉN-WAVE PROPAGATION*

John M. Wilcox, Alan W. DeSilva, and William S. Cooper, III

Lawrence Radiation Laboratory
University of California
Berkeley, California

May 10, 1961

INTRODUCTION

This paper reports an extension of previous experimental work with Alfvén waves.[1] We consider hydromagnetic waves propagating in a cylindrical plasma in a uniform axial magnetic field, as shown in Fig. 1. The copper tube is filled with highly ionized plasma by an electrically driven switch-on ionizing wave (by a process that will be described). After the tube is filled with plasma, a hydromagnetic wave is induced by a radial current flow from the small molybdenum electrode (at the left of Fig. 1) to the copper tube. The force produced by this radial current together with the static axial magnetic field displaces the plasma in the azimuthal (θ) direction, and a transverse wave is propagated in the axial direction, along magnetic field lines. The transient magnetic field associated with the wave is also in the azimuthal direction.

---

*Work performed under the auspices of the U. S. Atomic Energy Commission.

THEORY

The problem of torsional hydromagnetic waves propagating in a cylindrical plasma has been treated by a number of authors.[2-6] We shall follow Newcomb[3] and include finite conductivity. Azimuthal symmetry is assumed (see discussion on Generation of Waves). We will look for solutions to the equations in which the various field quantities have the form $F(r)e^{i(pz-\omega t)}$, i.e., are plane waves with sinusoidal time variation, propagating only in the z direction. Displacement current, viscosity, and plasma pressure are neglected.[7] The wave frequency (3×10^6 radians/sec for this experiment) is assumed low with respect to the ion-cyclotron frequency (typically 1.5×10^8 radians/sec for this experiment). We use rationalized MKS units in this discussion. We begin with the linearized form of Maxwell's equations, Ohm's law, and Newton's second law of motion:

$$\nabla \times \underset{\sim}{b} = \mu_0 \underset{\sim}{j}, \tag{1}$$

$$\nabla \times \underset{\sim}{E} = -\frac{\partial \underset{\sim}{b}}{\partial t} \tag{2}$$

$$\underset{\sim}{E} + v \times \underset{\sim}{B}_0 = \frac{\underset{\sim}{j}}{\sigma} \tag{3}$$

$$\rho_0 \frac{\partial \underset{\sim}{v}}{\partial t} = \underset{\sim}{j} \times \underset{\sim}{B}_0, \tag{4}$$

where $\underset{\sim}{b}$ is the oscillating magnetic field associated with the wave, $\underset{\sim}{j}$ is the current density associated with the wave, $\underset{\sim}{E}$ is the wave electric field, $\underset{\sim}{v}$ is the plasma velocity, $\underset{\sim}{B}_0$ is the static axial magnetic field supplied by external coils, ρ_0 is the plasma mass density, σ is the plasma conductivity, and μ_0 is the permeability of free space. Introducing $e^{-i\omega t}$ dependence and solving Eqs. (1) to (4) for the wave magnetic field b yields

$$\underset{\sim}{b} + \frac{1}{\mu_0 \omega^2 \rho_0} \nabla \times \left\{ \underset{\sim}{B}_0 \times \left[\underset{\sim}{B}_0 \times (\nabla \times \underset{\sim}{b}) \right] \right\} - \frac{1}{i\mu_0 \omega \sigma} \nabla \times \nabla \times \underset{\sim}{b} = 0. \tag{5}$$

This can be simplified to give

$$\nabla^2 b_z \hat{z} + \frac{\partial^2 \underset{\sim}{b}}{\partial z^2} - i\alpha \nabla^2 \underset{\sim}{b} - \nabla \frac{\partial b_z}{\partial z} + \frac{\omega^2}{V^2} \underset{\sim}{b} = 0, \tag{6}$$

where we have introduced the Alfvén velocity, $V = B_0/(\mu_0\rho)^{1/2}$, and the dimensionless parameter, $a = \omega/(\mu_0\sigma V^2)$; $\hat{z}$ is defined by $\hat{z} = \underset{\sim}{B}_0/B_0$.

The component of Eq. (6) that is perpendicular is $\hat{z}$ is

$$\frac{\partial^2 b_\perp}{\partial z^2} - ia\nabla^2 b_\perp - \nabla \frac{\partial b_z}{\partial z} + \frac{\omega^2}{V^2} b_\perp = 0, \tag{7}$$

where $\nabla_\perp$ is the perpendicular component of the gradient operator. Inserting the e^{ipz} dependence and rearranging, we have

$$\nabla_\perp^2 b_\perp + k_c^2 b_\perp + \frac{p}{a} \nabla_\perp b_z = 0, \tag{8}$$

where we define

$$k_c^2 = -p^2\left(1 + \frac{i}{a}\right)\frac{i}{a}\frac{\omega^2}{V^2}. \tag{9}$$

We are interested in the equation for b_θ, which comes from the azimuthal component of Eq. (8). In cylindrical coordinates this is

$$\frac{1}{r}\frac{\partial}{\partial r}\left(r\frac{\partial b_\theta}{\partial r}\right) - \frac{b_\theta}{r^2} + k_c^2 b_\theta = 0. \tag{10}$$

Then the general solution that is regular at $r = 0$ is

$$b_\theta = \sum_{n=1}^{\infty} b_{\theta n} J_1(k_{cn} r) \exp\left[i(p_n z - \omega t)\right], \tag{11}$$

where $J_1(k_{cn}r)$ is the first-order Bessel function, and n designates the mode of propagation. This type of wave is called a principal mode by Newcomb.[3] The $b_{\theta n}$ are constants determined by the form of the initial perturbation that induces the wave, and the k_{cn} are constants determined by a radial boundary condition. Experimentally, we shall find that one or two of the principal modes are sufficient to describe the observed distributions. The other wave quantities can be obtained from substitution in Eqs. (1) to (4):

$$v_\theta = - \sum_{n=1}^{\infty} \frac{p_n V^2}{\omega B_0} b_{\theta n} J_1(k_{cn} r) \exp\left[i(p_n z - \omega t) \right], \quad (12)$$

$$j_r = - \sum_{n=1}^{\infty} \frac{i p_n}{\mu_0} b_{\theta n} J_1(k_{cn} r) \exp\left[i(p_n z - \omega t) \right], \quad (13)$$

$$j_z = \sum_{n=1}^{\infty} \frac{k_{cn}}{\mu_0} b_{\theta n} J_0(k_{cn} r) \exp\left[i(p_n z - \omega t) \right], \quad (14)$$

$$E_r = \sum_{n=1}^{\infty} p_n \left[\frac{V^2}{\omega} - \frac{i}{\mu_0 \sigma} \right] b_{\theta n} J_1(k_{cn} r) \exp\left[i(p_n z - \omega t) \right], \quad (15)$$

$$E_z = \sum_{n=1}^{\infty} \frac{k_{cn}}{\mu_0 \sigma} b_{\theta n} J_0(k_{cn} r) \exp\left[i(p_n z - \omega t) \right]. \quad (16)$$

The attenuation of the various principal modes that is caused by ohmic losses will be needed for the analysis of the experimental results. If we set $p_n = k_n + i/L_n$, where k_n is the propagation constant, and L_n is the attenuation length for the nth principal mode (i.e., the distance in which a wave amplitude decreases to 1/e), then separating real and imaginary parts of Eq. (9) yields, in the case $a^2 \ll 1$, $a^2 (k_{cn} V/\omega)^4 \ll 1$,

$$L_n = \frac{2 \mu_0 \sigma k_n V^2}{\omega \left(k_{cn}^2 + \frac{\omega^2}{V^2} \right)} \quad (17)$$

and

$$k_n^2 = \frac{\omega^2}{V^2} = k^2. \quad (18)$$

Thus, to the order of approximation given above, the waves have no dispersion and no cutoff.

Analysis of Initial Disturbance into Radial Modes

The coefficients $b_{\theta n}$ appearing in Eqs. (11) through (16) are the amplitudes of the various radial modes. The relative amplitudes

of these modes are determined by the manner in which the wave is excited, i.e., in this case by the geometry of the driving electrodes. The fields produced by the source of excitation can be analyzed into the radial modes of the waveguide, which forms a complete orthogonal set.[8] Such an analysis is difficult for the case of finite conductivity, but for the case of no damping a simple analysis can be made. We shall make the analysis for no damping in order to find the relative amplitudes of the various modes at the excitation end, and then somewhat arbitrarily apply the damping of Eq. (17) to these modal amplitudes. In order to make the necessary expansion, one must know the boundary condition at the tube wall ($r = b$). This is the condition that determines the k_{cn}.

It has been found experimentally that the radial-wave current density j_r is zero at the tube wall (see Radial Distributions of Wave Magnetic Field). Equation (13) then shows the boundary condition to be $J_1(k_{cn}b) = 0$. This leads to something of an enigma, since the method of inducing the wave requires a current to flow to the wall. The explanation seems to be that a high-density current from an external source can penetrate the insulating layer which otherwise exists between the plasma and the wall. Experimental evidence on this point is presented later in this paper. For the present analysis, we approximate this state of affairs with the electrode structure shown in Fig. 2, taking at the end the limit as c approaches b.

The assumed boundary condition at the insulator surface at $z = 0$ is that the axial current density j_z is zero. The curl $\underset{\sim}{b}$ equation [Eq. (1)] then shows that $[(1/r)(\partial/\partial r)\, rb_\theta] + (1/r)(\partial b_r/\partial\theta) = 0$. If the input circuit has radial symmetry, then $\partial b_r/\partial\theta$ is zero, and the resultant equation shows that $b_\theta(r, 0)$ is proportional to $1/r$. At the electrode surfaces at $z = 0$, the tangential electric field is zero. If we assume zero damping, Eq. (18) then shows that the p_n are all equal. Comparison of the equations for E_r and b_θ [(Eqs. (11) and (15)] shows that b_θ is proportional to E_r, and is thus also zero at the electrode surfaces. We have then

$$b_\theta(r, 0) = \begin{cases} 0; & a < r;\ c < r < b \\ \dfrac{\mathcal{I}}{r} & a < r < c, \end{cases} \tag{19}$$

where $\mathcal{I}$ is a constant.

This function is now equated to Eq. (11) at $z = 0$, giving

$$b_\theta(r, 0) = \sum_{n=1}^{\infty} C_n J_1(k_{cn} r) , \tag{20}$$

where the time dependence has been omitted. To find $b_{\theta n}$, we multiply through on both sides by $J_1(k_{cn} r)\, r\, dr$, integrate over the interval $0 < r < b$, and go to the limit as c approaches b. Because of the orthogonality of the functions, only one term survives, and we obtain

$$C_n = \frac{-2\mathfrak{I}}{b^2} \quad \frac{J_0(k_{cn} b) - J_0(k_{cn} a)}{k_{cn} J_0^{\,2}(k_{cn} b)} . \tag{21}$$

The constant $\mathfrak{I}$ is determined by matching the vacuum magnetic field $b_{\theta vac}$ in the insulator to the magnetic field $b_\theta(r, 0)$ in the plasma. If we assume a symmetrical drive, the vacuum field is

$$b_{\theta vac} = \frac{\mu_0 I}{2\pi r} , \tag{22}$$

where I is the total current flowing to the electrode. Comparison of the preceding expression with Eq. (19) now shows that

$$\mathfrak{I} = \frac{\mu_0 I}{2\pi} . \tag{23}$$

This constant may also be expressed in terms of the applied voltage, V_0. It has already been shown that for zero resistivity and low frequency, $E_r(r)$ is proportional to $b_\theta(r)$, and hence goes as $1/r$. Integrating $E_r(r)$ between a and b gives the applied voltage, V_0, and we find that

$$E_r = \frac{V_0}{r \ln(b/a)} , \tag{24}$$

which is the same as the vacuum field. From Eqs. (11) and (15), the ratio of E_r to b_θ is V, so we obtain

$$b_\theta = \frac{V_0}{rV \ln(b/a)} \tag{25}$$

from which we have

$$\mathcal{K} = \frac{V_0}{V \ln(b/a)} \, . \tag{26}$$

Finally it should be noted that the input impedance is

$$Z_0 = \frac{V_0}{I} = \frac{\mu_0 V}{2\pi} \ln(b/a) \, , \tag{27}$$

which is just the characteristic impedance of a coaxial transmission line of inner and outer radii a and b, respectively, which is filled with a material of dielectric constant

$$K = \frac{\mu_0 \rho C^2}{B_0^2} \, , \tag{28}$$

where C is the speed of light in vacuum. This has previously been shown to be the appropriate dielectric constant for a magnetized plasma. [9]

The ratio of wave energy in any one mode to total wave energy is now easily shown to be

$$\frac{W_n}{W_T} = \frac{2}{b^2 \ln(b/a)} \left[\frac{J_0(k_{cn}b) - J_0(k_{cn}a)}{k_{cn} J_0(k_{cn}b)} \right]^2 \, . \tag{29}$$

In Table I we summarize some of the results of these calculations for conditions of this experiment. The second column shows the energy going into each of the first five modes, expressed as a percentage of total wave energy at the input end. The third column gives the peak value of $b_{\theta n}$ for each of these modes, where $\mathcal{K}$ has been calculated from Eq. (26), using for V_0 the observed value of 780 v. In the fourth column, we present the damping lengths (distance in which a wave field attenuates to 1/e of its initial value) calculated from Eq. (17). The value of resistivity used

Table I

Some results of the modal analysis

Mode number n	Initial energy (% of total wave energy)	Initial peak value of b_θ at driving end (gauss)	Damping length, L (cm)	Peak value of b_θ after one transit (74 cm) (gauss)
1	79	+476	107	238
2	7	-188	32	17.5
3	0.7	- 74	15	0.5
4	4.3	-206	9	0.05
5	2.5	+176	6	---

was 3.19×10^{-4} ohm-meters and was experimentally determined by measuring the attenuation of a wave that had traveled far enough so that only the lowest mode was present. Thus the damping length for the n=1 mode is experimentally determined, and the others are calculated using the same value of resistivity. In the last column we have applied the damping of column four to the amplitudes in the third column to obtain the wave amplitudes after one transit through the tube.

The lowest mode is excited most strongly (79% of the wave energy goes into this mode), and has considerably less attenuation than the higher modes. After the wave has made one transit through the tube, the amplitude of the second mode is only 7% of the amplitude of the lowest mode, and the higher modes are present to a negligible extent.

EXPERIMENTAL METHOD AND RESULTS

Plasma Preparation

The geometry of the hydromagnetic waveguide is shown in Fig. 1. A copper cylinder 86.4 cm long and 14.6 cm in diameter is placed in a uniform axial magnetic field of 16.0 kgauss and filled with hydrogen gas to a pressure of 100 μ. The ionizing current is supplied by a lumped-constant pulse line, so that the current of about 9000 amp is nearly constant during the period of ionization. Conditions are such that the potential of about 4500 v applied to the tube is also nearly constant, as shown in Fig. 3. This pulse line is connected between the electrode and the copper cylinder through an 0.8-ohm series resistance and an ignitron switching tube. When the current from this source is switched on, a local breakdown occurs in the gas at the end of the tube, after which a sharply defined ionizing wave travels through the gas. This wave shows similarities both to a switch-on shock wave and to a detonation wave and is referred to as a switch-on ionization wave. The wave travels typically at 5 cm/μsec, and its front has been shown by magnetic probes and local wall-current probes to rise in about 0.5 μsec, corresponding to a thickness of the current layer of 2 to 3 cm. Note that since the current is forced by external circuitry to flow to the wall, the restriction mentioned in the theory section (j_r at the wall is zero) does not

apply here. Figure 4 shows on the lower trace the voltage at an electrode (not shown in Fig. 1) placed coaxially in the end plate opposite the driving end and connected to the tube wall through a 0.3-ohm resistor. This voltage remains at zero during the time the wave is traveling through the tube, then rises abruptly at the time the wave arrives. The progress of the wave down the tube can be observed by noting its time of arrival at each of five radial-current probes (Fig. 5) mounted in the cylinder wall. The radial-current probe consists of a 0.25-in. diam. section of the tube wall which is electrically isolated and connected to the adjacent cylinder through a 0.85-ohm resistance. The position of the wavefront as a function of time is shown in Fig. 6.

If the ionizing current continues to flow after the tube is filled with plasma, a sudden increase in the intensity of emission lines from materials associated with the pyrex end plates is observed spectroscopically. Therefore our practice is to short-circuit (crowbar) the ionizing current as soon as the switch-on ionizing wave has filled the tube with plasma. This procedure is subject to one conspicuous exception, described later in connection with reflection from a copper end plate.

The ion density along a column of plasma 5 cm in diameter coaxial with the cylinder wall has been determined as a function of time.[10] This is accomplished by measuring the first-order Stark broadening of the first three Balmer lines (H_α, H_β, H_γ), using a monochromator to scan the lines. Cross-plots give the line shape as a function of time, and the curves are compared with the theory of Griem, Kolb, and Shen[11] to find the ion densities. The result is that at the time the ionizing wave reaches the end of the tube, the ion density is $>5\times10^{15}$ cm^{-3}, corresponding to 80 to 100% ionization of the original neutral hydrogen gas present. The ion density decays by a factor of two in about 150 μsec. The ion density as a function of time is shown in Fig. 7. At the time the hydromagnetic wave experiments are performed, the ion density corresponds usually to >80% of the density of original neutral gas. The amount of neutral gas present at this time has not been measured. The temperature of the plasma at this time has been estimated from observed Alfvén-wave damping to be at least 10^4 °K.

Generation of Waves

A torsional hydromagnetic wave is induced in the plasma by discharging a 0.2-μf capacitor between the center electrode and the copper cylinder after the tube has been filled with plasma. For this work, the capacitor is critically damped so that only a single pulse of current flows. The current pulse is roughly a half sine wave, 0.8 μsec long. The resulting wave has been detected with small magnetic probes, which consist of a coil of 75 turns of wire on a 1-mm-diam. form. The coils are mounted inside reentrant glass tubes fused onto the insulator at the receiving or driving end of the waveguide.

Our theoretical analysis postulates an azimuthally symmetrical wave propagation. The coaxial driving-electrode system has this property, and the copper cylinder was carefully aligned with the axial magnetic field by a method which has been previously reported.[12] The azimuthal symmetry was measured experimentally with four magnetic probes disposed 90 deg apart on the same base circle. A random shot-to-shot variation of 10 to 20% was observed in individual probe signals, but the average of several shots gave azimuthal symmetry to within a few percent.

Reflections

An important check on the interpretation of these waves is provided by observation of reflections from various types of boundaries.[13] These reflections have been observed from an insulating end plate, from a conducting end plate, and from a plasma-neutral gas interface. The phase relationships of reflected-to incident-wave fields at the boundary surface can be predicted easily by an examination of the wave fields in Eqs. (11) through (16). One can measure the wave magnetic field b_θ and the voltage V between a center coaxial electrode (of radius a) and the tube (of radius b), where

$$V = \int_a^b E_r \, dr.$$

We would thus like to analyze the phase relations to be expected for b_θ and E_r. For an insulating boundary at $z = z_0$, assuming no accumulation of charge, we have $j_z(r, z_0) = 0$. Then from Eq. (14) one

can see that $b_{\theta n}$ must reverse its algebraic sign in the reflected wave. Also p_n always changes sign in the reflected wave, since this wave is propagating in the negative direction. Then from Eq. (11) we can see that b_θ changes phase on reflection, since it is proportional to $b_{\theta n}$, which changes sign. From Eq. (15) we note that E_r is proportional to the product of $b_{\theta n}$ and p_n (both of which change sign), and therefore E_r does not change phase on reflection.

For a conducting boundary at $z = z_0$, the condition is $E_r(r, z_0) = 0$. Then by a similar argument we find that E_r changes phase on reflection and that b_θ does not.

Figure 8 shows V (top trace) and b_θ (bottom trace) for the case in which a wave is reflected from a pyrex end plate at the far end of the tube. The voltage V is measured between the molybdenum electrode and the copper tube at the end of the tube (left-hand side of Fig. 1), and the wave magnetic field is measured with a magnetic probe 13 cm from the driving end (not shown in Fig. 1). The first signal is due to the initial wave, and then, after a time delay corresponding to two transits of the tube with a velocity equal to the Alfvén velocity, the signal from the reflected wave appears. The voltage (E_r) reflects in-phase and the magnetic field (b_θ) out-of-phase, as expected.

We next inserted a copper end plate in order to demonstrate reflections from a conducting boundary. The unexpected results shown in Fig. 9 were obtained; i.e., the phase relations are appropriate to a reflection from an insulating boundary. Apparently the plasma had become electrically isolated from the copper end plate, i.e., an insulating layer had formed at the wall. The source of this layer is unknown, but it seems most reasonable to believe that it is just due to a simultaneous drop in temperature and electron density in the immediate vicinity of the wall, which is in effect a low-temperature heat sink. If this hypothesis is correct, one might reasonably expect that a high-density current flowing from the plasma to the copper plate would inhibit the formation of an insulating boundary layer and thus maintain electrical contact between plasma and copper. If the ionizing current from the pulse line is <u>not</u> crowbarred after the tube has been filled with plasma, this current continues to flow axially through the tube and into the copper plate. We therefore reflected a wave from the copper end plate while the ionizing current was flowing and obtained the results shown in Fig. 10.

The electric field E_r now changes phase on reflection and the magnetic field b_θ does not, as predicted for a conducting boundary. We shall return in the next section to the subject of the insulating layer surrounding a quiescent plasma.

Reflection of Alfvén waves from a plasma-neutral gas interface has also been observed. If the ionizing current is turned off (crowbarred) when the ionizing wave is part way down the tube, part of the tube is filled with a highly ionized plasma and the rest is filled with neutral gas (or at least gas with a very low degree of ionization). Under such conditions the Alfvén-wave reflections shown in Fig. 11 were obtained, which have the expected phase relations for a nonconducting boundary. In the previous three cases, attenuation in the body of the plasma could explain the difference in incident-and reflected-wave amplitudes, but in this case, the difference in amplitudes is too large and indicates a lossy reflection. The ionizing current was stopped when the ionizing wave had just reached a radial current probe located 58 cm from the driving end of the tube. We waited 10 μsec for the ionizing current flow to cease and then induced the Alfvén wave. During this waiting time, the interface probably moved on down the tube because of the plasma pressure. Using the Alfvén velocity measured under similar conditions when the tube was full of plasma, and the wave transit time measured from Fig. 11, one calculates that the reflection occurs from an interface located 68 cm from the driving end of the tube, in reasonable agreement with the estimate given above. Also, a magnetic probe near the receiving end of the tube (in the neutral gas) detected no wave signal. Thus reflection of Alfvén waves from a plasma-neutral gas boundary seems to be established. This phenomenon may be of particular interest in some astrophysical and geophysical problems.

Radial Distribution of Wave Magnetic Field

The radial distribution of the azimuthal magnetic field b_θ associated with the wave has been measured with magnetic probes. Six probes were used, disposed near the receiving-end insulator at various radii. A typical probe container is shown at the right side of Fig. 1. The result of this measurement is displayed in Fig. 12.

The solid curve is experimental data for a wave induced 20 μsec after the ionizing current was crowbarred.

The observed b_θ becomes zero at the tube wall. Reference to Eqs. (11) and (13) shows that b_θ and j_r have the same radial dependence. Therefore the observation indicates that no radial currents flow to the tube wall, as was previously noted in the section on theory. This observation was found to be true independently by looking for wall currents with the radial-current probes. At first glance, the result is surprising, since the conductivity of the copper is much higher than that of the plasma, and since the method of inducing the wave requires a current to flow to the wall. However, for the reasons discussed in the preceding section, the electrical conductivity in the plasma adjacent to the wall may be low, isolating the plasma from the wall. The same distribution of b_θ was observed with either polarity of driving current, so that this effect does not seem to be associated with the well-known anode sheath, which is sometimes observed in discharges where the current flow to a boundary surface is perpendicular to the static magnetic field.

The experimentally determined boundary condition that radial current is zero at the wall leads to the theoretical prediction for $b_\theta(r)$ which is shown as a dashed line in Fig. 12. This curve is calculated from the information given in Table I. The zero of the Bessel function was taken to be 4 mm inside the physical wall, to better match the experimental data; this distance may be interpreted as roughly indicating the thickness of the nonconducting layer of gas. The prediction for the amplitude of the received wave, based on the observed voltage at the driving end of the tube and the measured damping length, agrees within 15% with the measured amplitude. Thus within this accuracy one can follow the flow of energy from the wave-generating capacitor through the hydromagnetic waveguide.

The radial distribution of the wave magnetic field b_θ was also measured for a wave that had reflected from the receiving end of the tube and then from the driving end, i.e., the wave had made three transits of the tube. The result is displayed in Fig. 13. The dashed curve is the theoretical prediction for the lowest principal mode, also calculated from the information in Table I.

ACKNOWLEDGMENTS

We wish to thank Dr. C. M. Van Atta and William R. Baker for interest in and encouragement of this work. Dr. William A. Newcomb made his unpublished analysis of hydromagnetic waveguides available to us. We wish to thank Drs. Wulf B. Kunkel, Theodore G. Northrop, and Klaus Halbach for commenting on the manuscript. Gerald V. Wilson, Louis A. Biagi, Peter R. Forman, and Pierre F. Pellissier gave us able assistance in the experimental work.

REFERENCES

[1] ALLEN, T. K., et al., Phys. Rev. Letters 2 (1959) 383; WILCOX, J. M., et al., Phys. Fluids 3 (1960) 15.

[2] BAÑOS, A., Proc. Roy. Soc. (London) 233 (1955) 350.

[3] NEWCOMB, W. A., in Magnetohydrodynamics, Stanford University Press, Stanford, California (1957) 109.

[4] LEHNERT, B., Nuovo cimento, Suppl. 13, No. 1 (1959).

[5] GAJEWSKI, R., Phys. Fluids 2 (1959) 633.

[6] SCHMOYS, J., et al., Phys. Fluids 3 (1960) 473.

[7] For the solution which is obtained, the divergence of v is zero, so pressure effects are absent to first order.

[8] GOULD, R. W., Space Technology Laboratories Inc. Report STL/TR/60-0000-09143 (1960).

[9] SPITZER, L., The Physics of Fully Ionized Gases, Interscience Publishers, Inc., New York (1956) 35.

[10] COOPER, W. S., III, et al., Ion Density Measurements in a Decaying Hydrogen Plasma, Lawrence Radiation Laboratory Report UCRL-9509, March 1, 1961.

[11] GRIEM, H. R., et al., Phys. Rev. 116, (1959) 4; idem, NRL Report 5455, March 4, 1960.

[12] DE SILVA, A. W., et al., Rev. Sci. Instr. 31, (1960) 455.

[13] Reflection of plasma Alfvén waves has been observed independently by Shigeo Nagao and Teruyuki Sato, Tohoku University, Sendai, Japan (private communication).

FIGURE LEGENDS

Fig. 1. Experimental geometry.

Fig. 2. Electrode arrangement assumed for modal analysis.

Fig. 3. Oscilloscope traces showing ionizing conditions. The top trace is voltage on the driving coaxial electrode at 2400 v/cm and the bottom trace is current from the pulse line at 10^4 amp/cm. The horizontal scale is 10 μsec/cm. The current was crowbarred 22 μsec after the voltage was first applied. A single-pulse hydromagnetic wave was induced 48 μsec after the voltage was first applied.

Fig. 4. Oscilloscope traces showing arrival of ionization front. The top trace is the voltage on the driving coaxial electrode at 1000 v/cm; the bottom trace is the voltage on the receiving coaxial electrode at 1000 v/cm. The horizontal scale is 10 μsec/cm. The axial magnetic field is 10 kgauss. The abrupt rise of the received voltage is evidence for a well-defined ionization front. Note that the information that the front has reached the load at the receiving end (0.33 ohm, not shown in Fig. 1) requires one Alfvén transit time (2.8 μsec) to reach the driving end, at which time the driving voltage decreases somewhat.

Fig. 5. Geometry of the radial-current probe. The 1/4-in.-diam button is connected to the adjacent wall through six parallel 5-ohm resistors. The maximum voltage drop is less than 1 v.

Fig. 6. Position of the ionization front vs time, as measured with radial current probes. The 16-kgauss axial magnetic field resulted in a shorter transit time for the front than is the case shown in Fig. 3.

Fig. 7. Observed time dependence of the ion density. Errors (not shown) in the experimental points are estimated to be $\pm 1.0\times10^{15}$ cm^{-3} late in the decay period. The solid line is a least-squares fit, assuming the decay rate to be proportional to the square of the ion density. The dashed line assumes an exponential decay.

Fig. 8. Oscillogram showing reflection from a pyrex end plate. The upper trace is the voltage measured at the driving end of the tube between the cylinder and coaxial electrode at 100 v/cm. The lower trace is the azimuthal magnetic field, measured by a probe 13 cm from the driving end with a sensitivity of 34 gauss/cm. The sweep speed is 1 μsec/cm. The first pulse is the induced wave, and the first reflection occurs about 3.5 μsec later, on the voltage trace, corresponding to two transits through the tube at the Alfvén speed. The voltage reflects in phase, the magnetic field out of phase, in accord with theory for a nonconducting boundary.

Fig. 9. Oscillogram showing reflection from a copper plate 30 μsec after the plasma has started to decay. Traces are as in Fig. 8, with upper trace at 250 v/cm and lower trace at 50 gauss/cm. The phase of the reflected fields is the same as for a nonconducting boundary, indicating that the copper wall is isolated from the plasma.

Fig. 10. Oscillogram showing reflection from a copper plate with ionizing current still flowing to the plate. Traces are as in Fig. 8, with the upper trace at 250 v/cm and the lower trace at 68 gauss/cm. The electric field has reflected out-of-phase and the magnetic field in-phase, in agreement with theory for a conducting boundary.

Fig. 11. Oscillogram showing reflection from an interface between plasma and neutral gas. The upper trace is the voltage on the end electrode at 250 v/cm, and the lower trace is the magnetic field at 70 gauss/cm. The phases indicates a nonconducting boundary at reflection. The small amplitude of the reflected signal indicates a lossy reflection.

Fig. 12. The radial distribution of the wave magnetic field b_θ, measured near the receiving end of the tube after the wave has made one transit (Z = 74 cm). The dashed curve is the theoretical distribution from Table I, and the solid curve is the measured distribution.

Fig. 13. The radial distribution of the wave magnetic field b_θ, measured near the receiving end of the tube after the wave has made three transits of the tube (i.e., two reflections; Z = 247 cm); 20 μsec after crowbar. The dashed curve is the theoretical distribution for the lowest mode ($J_1(k_{cn}r)$, based on the predictions of Table I.

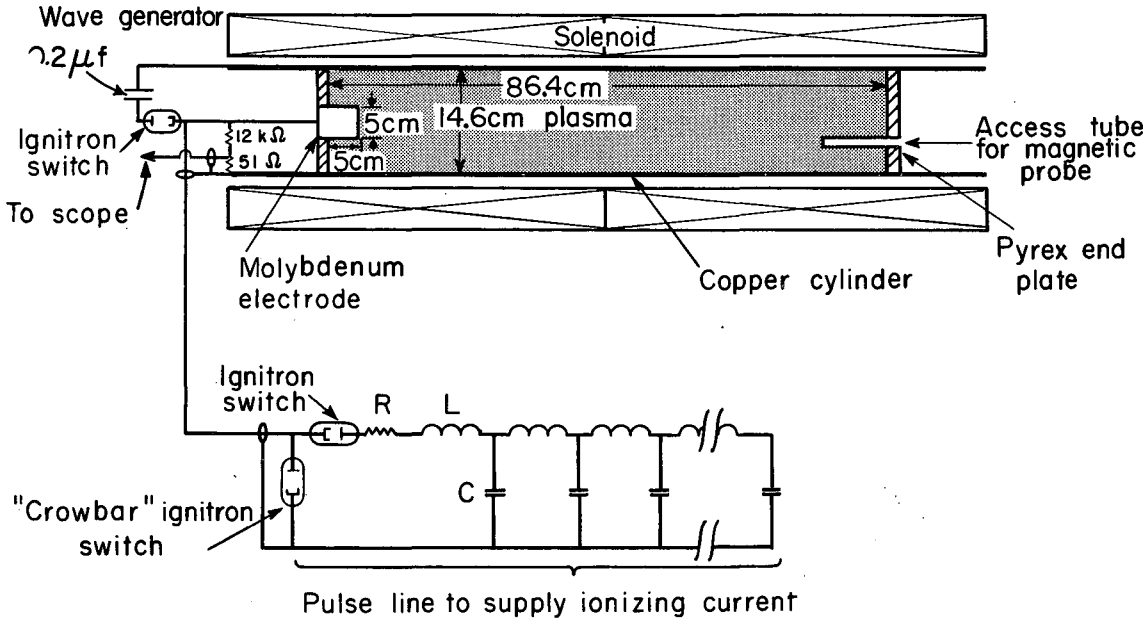

MU-22165

Fig. 1

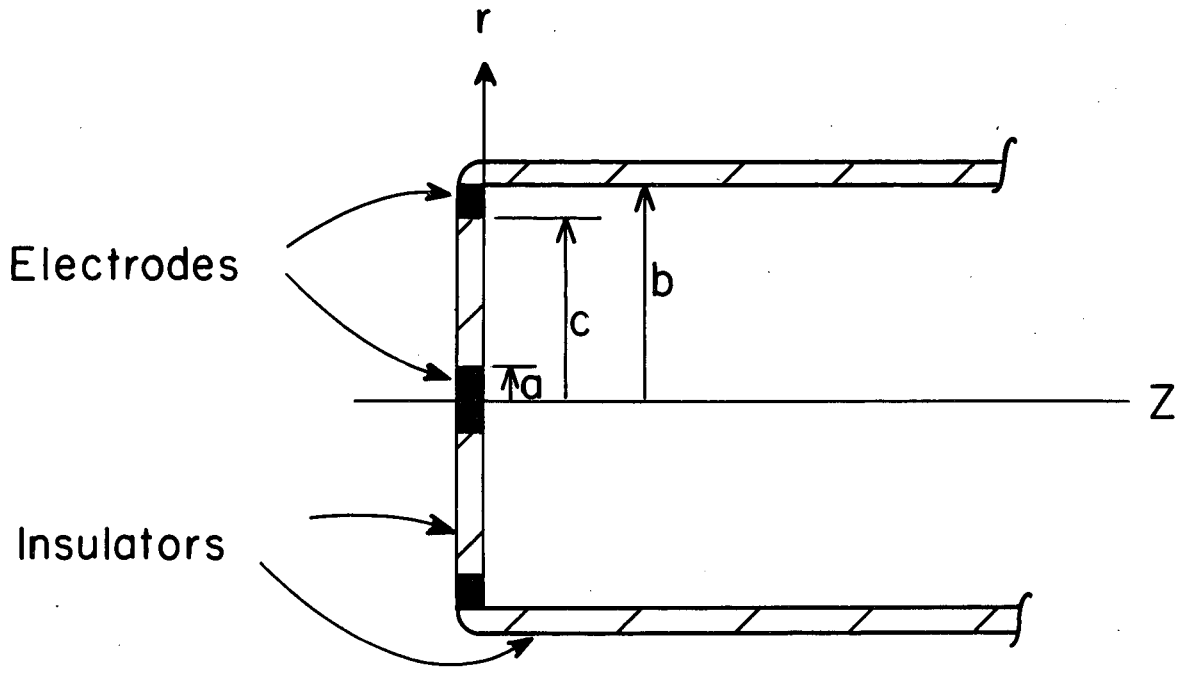

Fig. 2

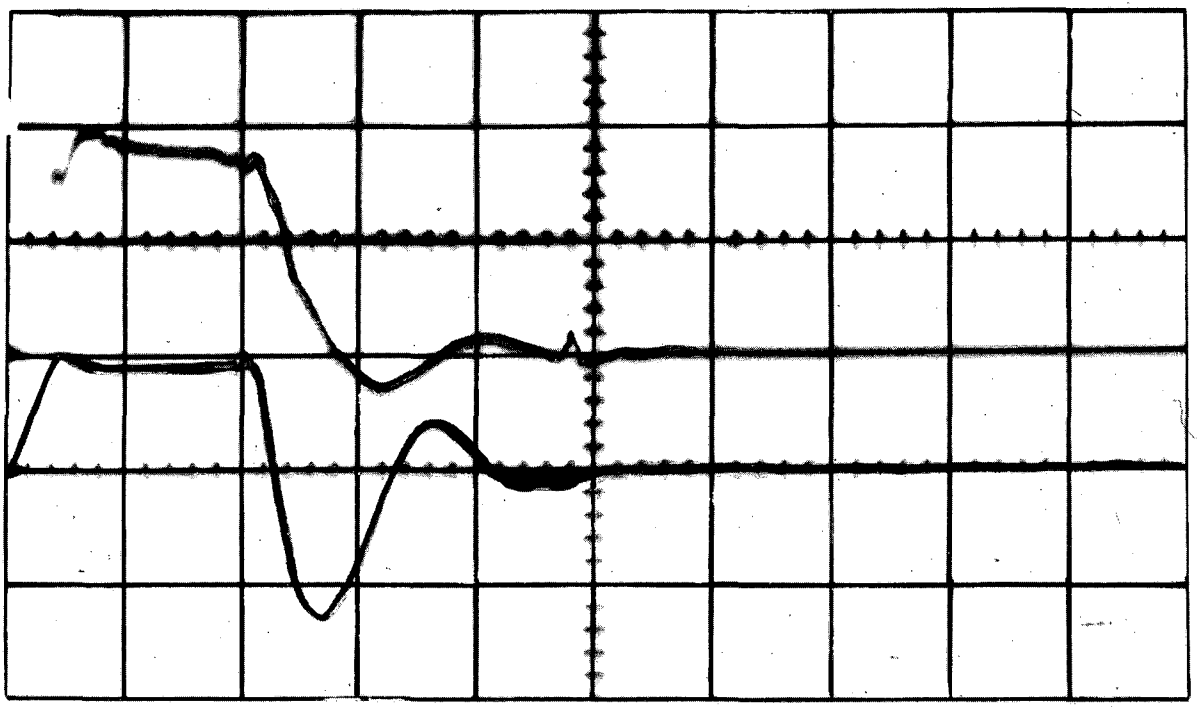

ZN-2492

Fig. 3

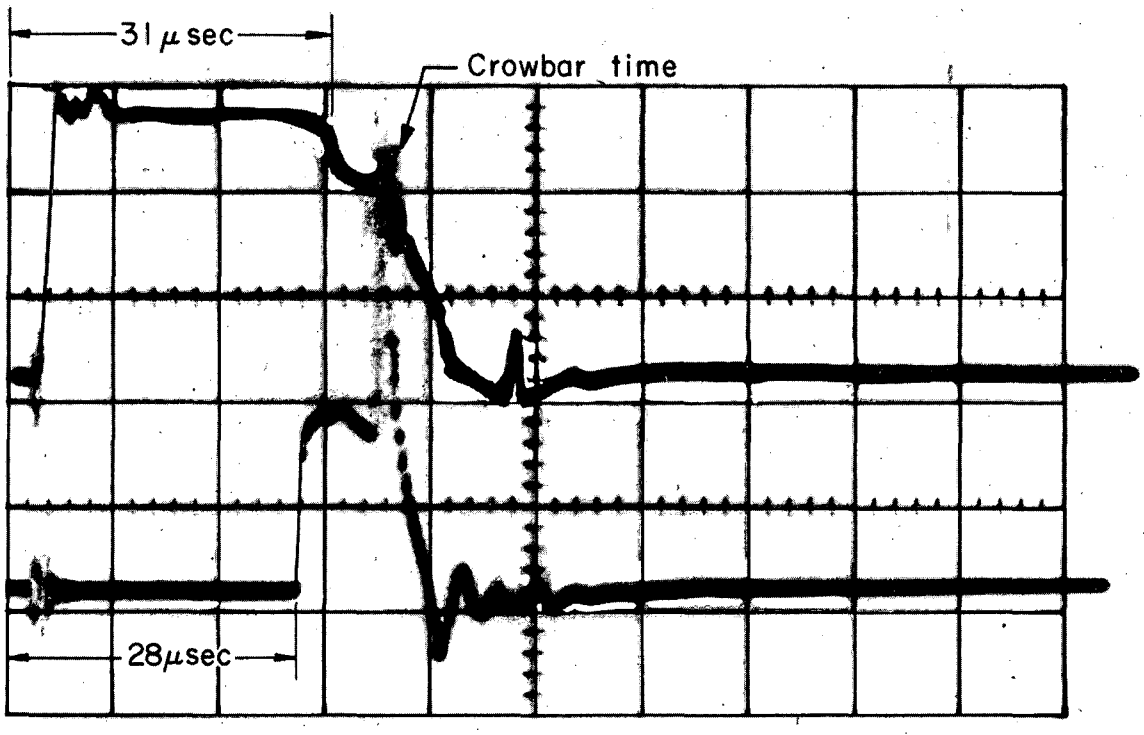

ZN-2493

Fig. 4

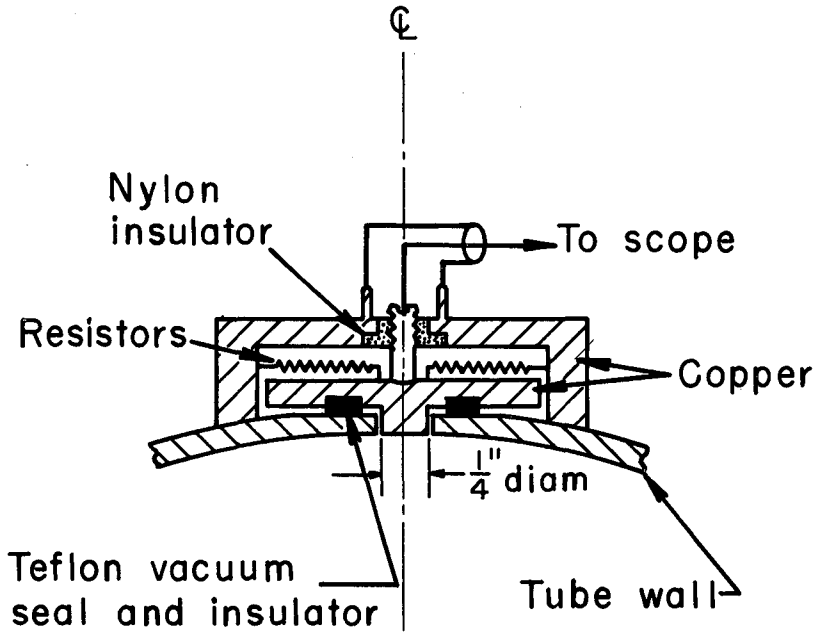

MU-20358

Fig. 5

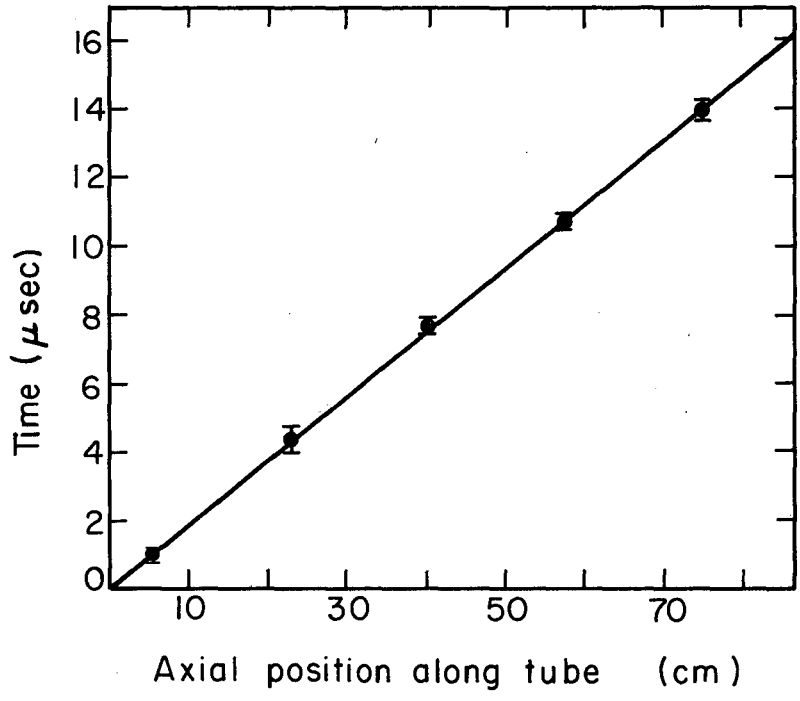

MU-20359

Fig. 6

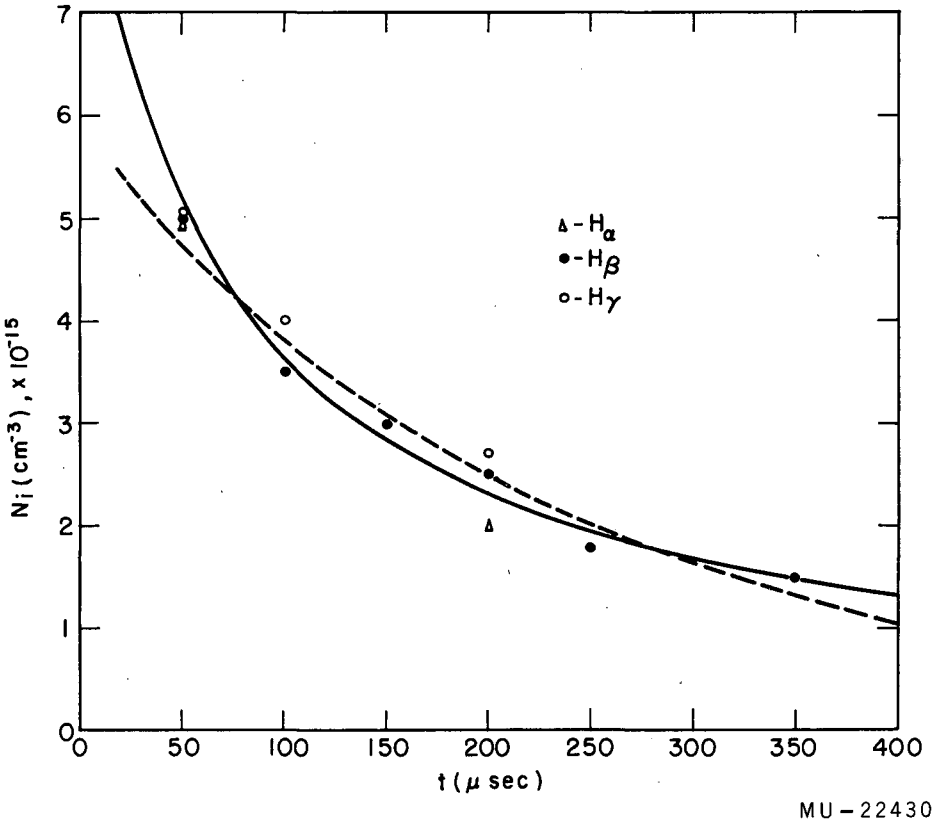
7
6
5
4
3
2
1
0
0
50
100
150
200
250
300
350
400
N_i (cm^{-3}), x 10^{-15}
t (μ sec)
Δ - H_α
• - H_β
○ - H_γ
MU-22430

Fig. 7

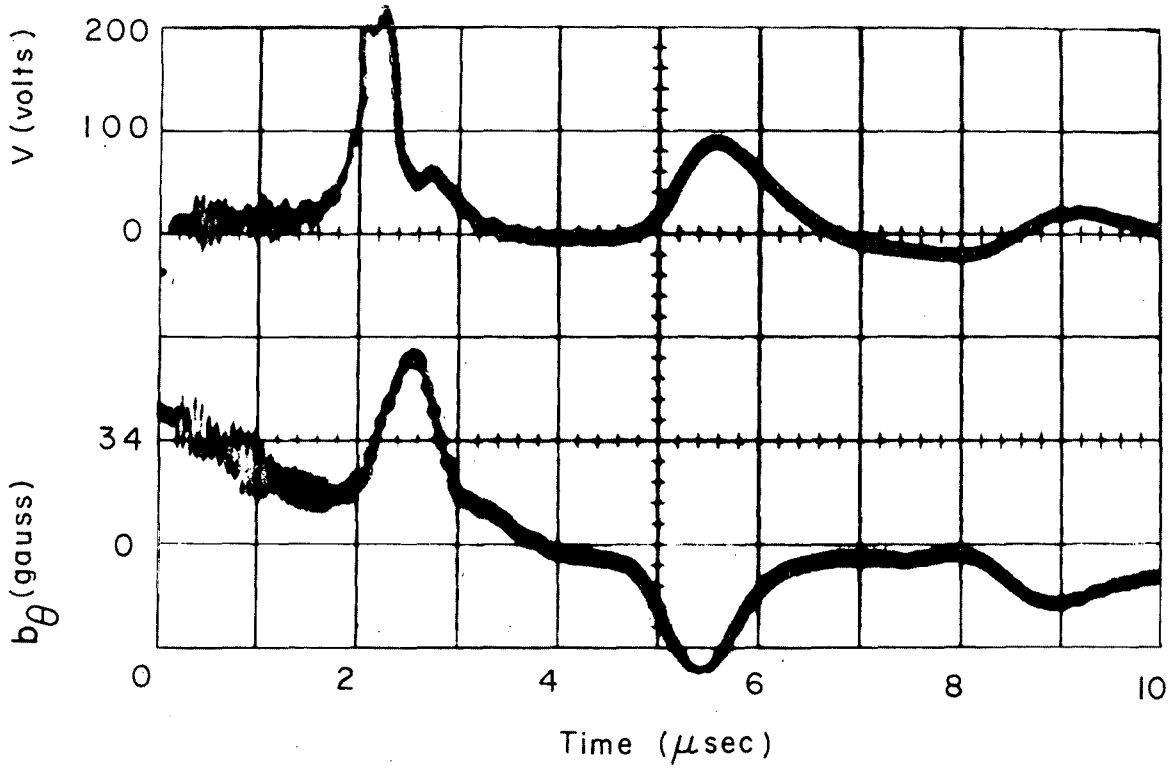

ZN-2622

Fig. 8

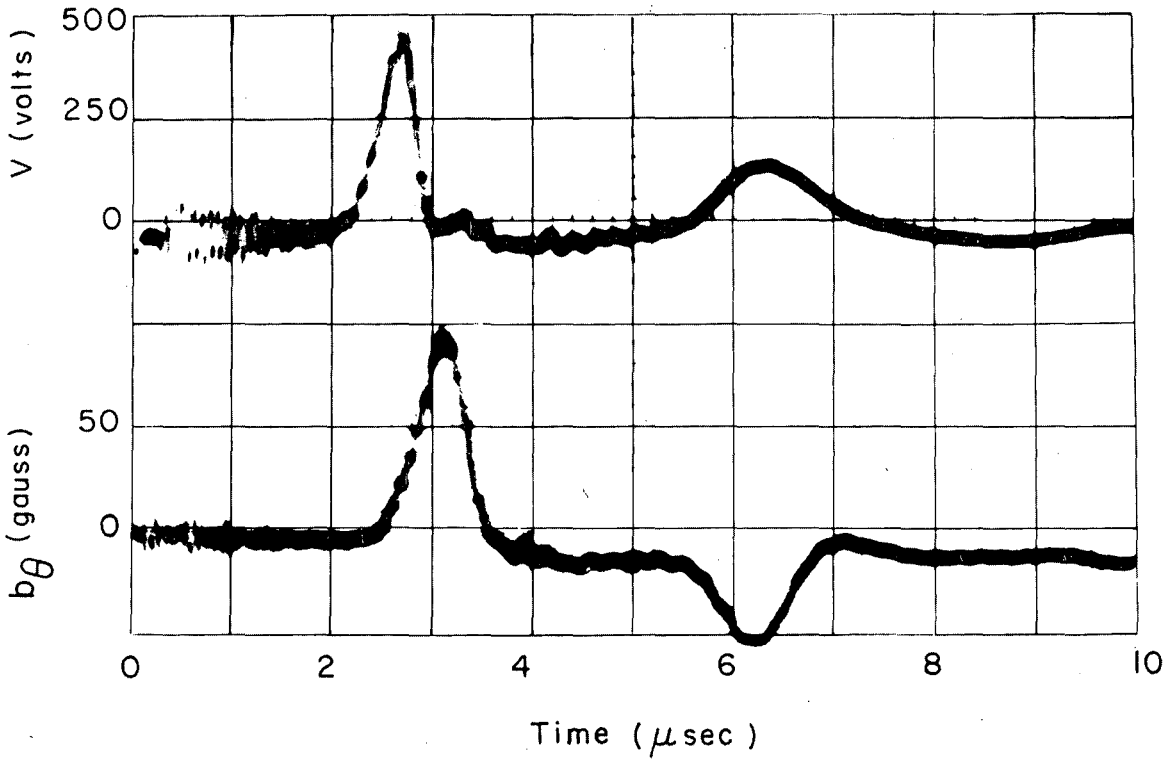

ZN-2623

Fig. 9

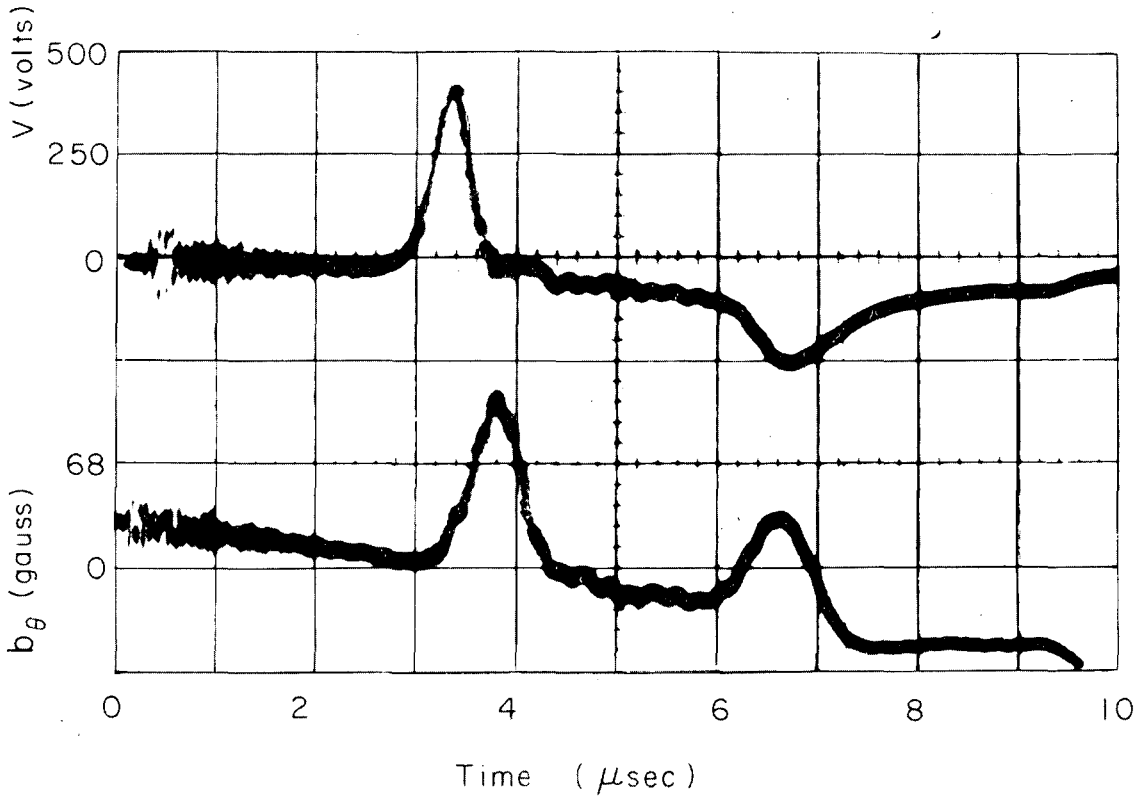

ZN-2620

Fig. 10

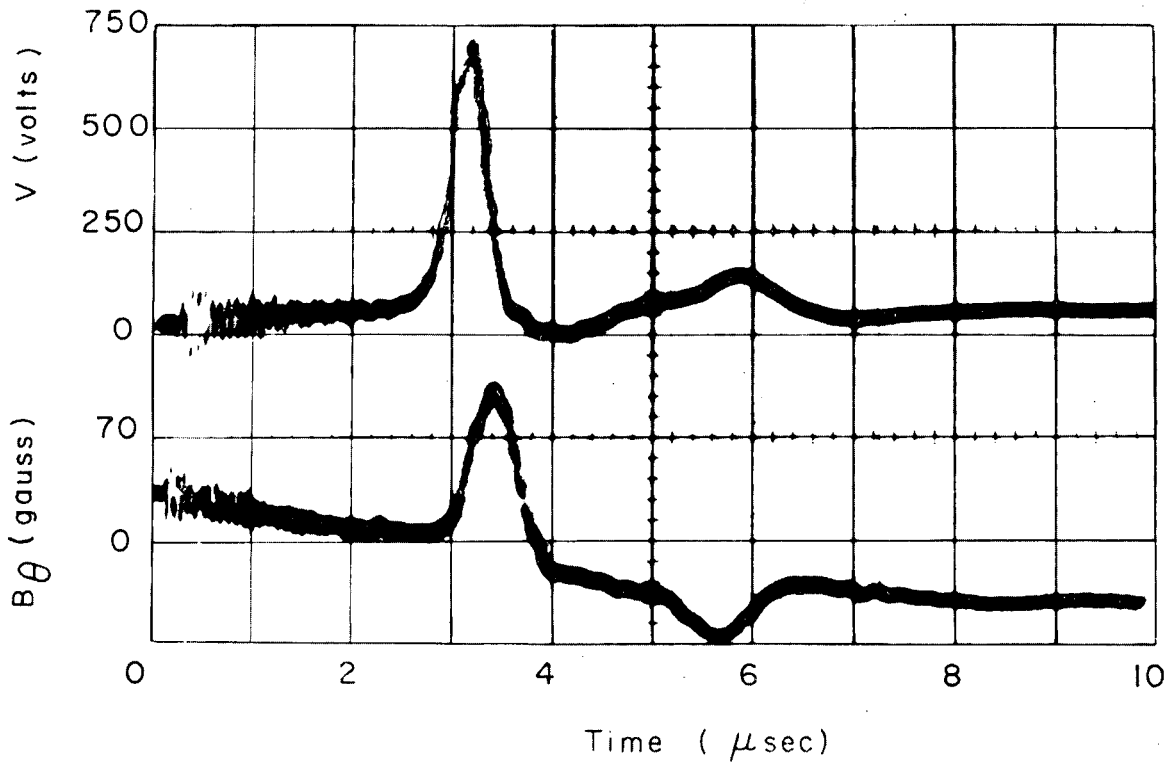

ZN-2621

Fig. 11

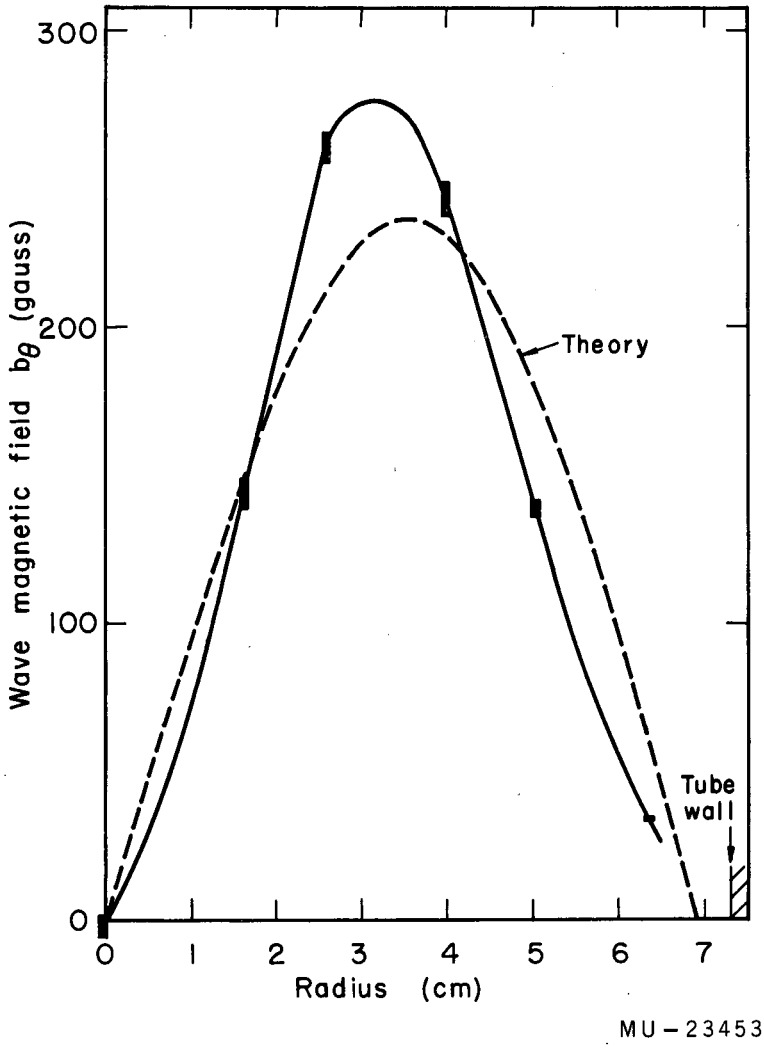
300
200
100
0
Wave magnetic field b_θ (gauss)
Theory
Tube wall
0
1
2
3
4
5
6
7
Radius (cm)
MU-23453

Fig. 12

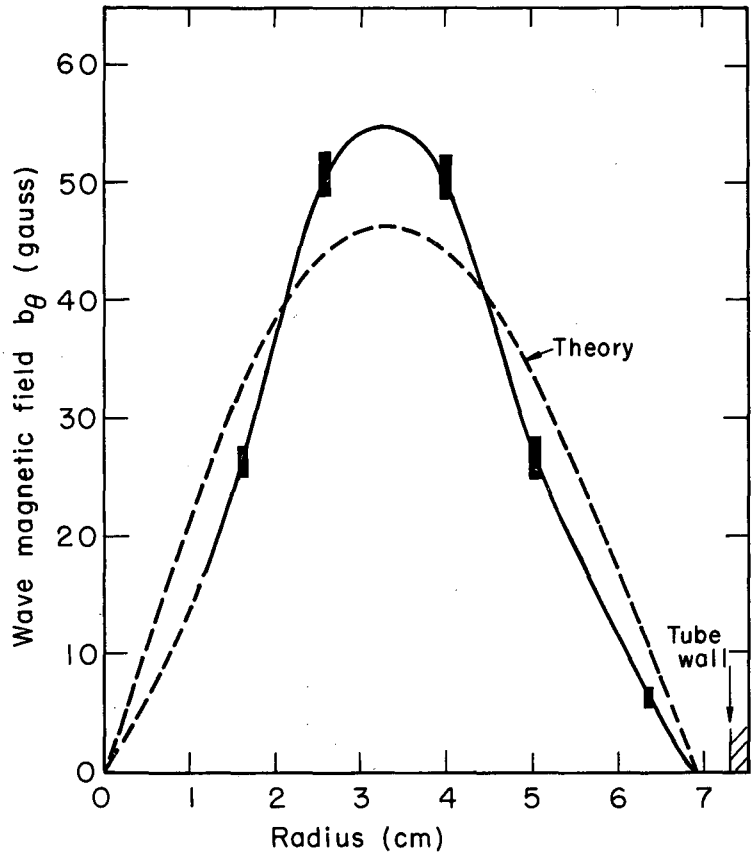
Wave magnetic field b_θ (gauss)
60
50
40
30
20
10
0
0
1
2
3
4
5
6
7
Radius (cm)
Theory
Tube wall
MU-23452

Fig. 13